Liquid Crystals
Publication details, including instructions for authors and subscription information:
http://www.informaworld.com/smpp/title~content=t713926090

New compounds with a TGBA-TGBC-SmC* phase sequence

Miroslav Kašpar[a]; Vladimíra Novotná[a]; Milada Glogarová[a]; Věra Hamplová[a]; Damian Pociecha[b]
[a] Institute of Physics, Academy of Sciences of the Czech Republic, Na Slovance 2, CZ-182 21, Czech Republic [b] Chemistry Department, University of Warsaw, Al. Zwirki i Wigury 101, 02-089, Poland

Online publication date: 11 February 2010

To cite this Article Kašpar, Miroslav , Novotná, Vladimíra , Glogarová, Milada , Hamplová, Věra and Pociecha, Damian(2010) 'New compounds with a TGBA-TGBC-SmC* phase sequence', Liquid Crystals, 37: 2, 129 — 137
To link to this Article: DOI: 10.1080/02678290903419053
URL: http://dx.doi.org/10.1080/02678290903419053

Liquid Crystals,
Vol. 37, No. 2, February 2010, 129–137

Taylor & Francis
Taylor & Francis Group

New compounds with a TGBA-TGBC-SmC* phase sequence

Miroslav Kašpar[a], Vladimíra Novotná[a]*, Milada Glogarová[a], Věra Hamplová[a] and Damian Pociecha[b]

[a]*Institute of Physics, Academy of Sciences of the Czech Republic, Na Slovance 2, CZ-182 21 Prague 8, Czech Republic;* [b]*Chemistry Department, University of Warsaw, Al. Zwirki i Wigury 101, 02-089 Warsaw, Poland*

(Received 1 July 2009; accepted 15 October 2009)

A new series of lactic acid derivatives has been prepared with molecular cores consisting of two laterally substituted biphenyls connected by an ester group. The compounds exhibited the TGBA phase in a broad temperature range. In addition, for some compounds, a narrow blue phase was found above the TGBA phase on cooling from the isotropic phase. Except for the compound with the shortest chain, the TGBC phase appeared below the TGBA phase. The low temperature SmC* phase existed within the interval up to 80 K, including the overcooled state, which was down to room temperature. In the compounds studied a strong pre-transitional phenomenon took place manifested as a broad peak on the differential scanning calorimetry plot in the isotropic phase. The phases were established on the basis of a planar sample and free-standing film microscope observation. Small angle X-ray diffraction measurements provided information about layer spacing, *d*, and confirmed the phase assignment. Dielectric spectroscopy revealed the soft and Goldstone modes in the respective TGBA and SmC* phases.

Keywords: ferroelectric liquid crystals; TGBA phase; TGBC phase; dielectric spectroscopy; lactic acid derivatives

1. Introduction

Twist grain boundary (TGB) phases are still the subject of intense studies. The appearance of these frustrated phases results from competition between chiral forces and the tendency of molecules to pack effectively into layers. The model of the TGBA (TGBC) phase [1] presumes small blocks with a layered SmA (SmC*) structure separated from each other by grain boundaries of screw dislocations [1, 2]. The reason for the TGB phase's appearance is that the direct cholesteric-smectic phase transition cannot occur in a continuous way since the cholesteric twist of the director is not compatible with smectic layering. TGB phases exhibit distinct structural features, that is, smectic layers and a helical superstructure with its axis parallel to the smectic layers [3–5]. While the structure of the TGBA phase seems to be quite well understood, the character and properties of its tilted variants are still a subject of intense debate. The tilted TGBC phase was first experimentally proved by Nguyen *et al.* [6]. Several types of TGBC phase with different local smectic structures have been found [7–9]. In the TGBC phase the molecular tilt in the smectic blocks is uniform, while in the TGBC* phase the blocks are filled by the SmC* phase modulated in a direction perpendicular to the normal block. In Lukyanchuk [10] and Galerne [11], the Renn and Lubensky model was modified on the basis of a calculation of elastic interactions for the TGBC* phase. Dielectric studies of TGB phases are scarce [12–14], and questions still exist concerning the temperature behaviour of dielectric response and the origin of observed modes. Ismaili *et al.* [15] have observed the soft mode in the TGBA phase and the Goldstone mode in the TGBC phase, the dielectric strength of both modes being much lower and the relaxation frequency much higher compared with those typically found in the SmC* and SmA phases. They explained this difference on the basis of a modified Landau free energy, taking into account the elastic strain connected to the anchoring at the grain boundaries and the dimensions of the smectic blocks.

Liquid crystals incorporating lactate units frequently exhibit unusual mesomorphic properties, for example, the presence of the re-entrant smectic C phase [16]. However, the effect of the number of chiral centres and/or their configuration (S, R) on the occurrence of mesophases has still not been clarified. Recently, mesogens with a naphthalene core and lactic unit in the chiral chain that exhibit the TGBA phase have been described [17]. Nevertheless, the relationship between the structure and formation of the TGB phases is still unknown and their physical properties have not been systematically studied due to the rarity of these phases and their existence in a narrow temperature interval.

While designing new liquid crystal molecules, the fact that their mesogenic behaviour is influenced not only by the structure of the core but also by the chiral part of the molecule should be borne in mind. Application of a single lactate unit as a basis of the chiral part has yielded many materials with a broad ferroelectric phase [18]. Materials with two lactate units have been described in several papers [19–21]

*Corresponding author. Email: novotna@fzu.cz

ISSN 0267-8292 print/ISSN 1366-5855 online

DOI: 10.1080/02678290903419053
http://www.informaworld.com

and among them some compounds exhibiting the antiferroelectric phase were reported. Recently, a series of ferroelectric liquid crystalline materials with two chiral centres, one composed of the lactate unit, have been synthesised [19]. These compounds show an extremely broad temperature interval of the TGB phase, which probably occurs due to a strong chiral force of this type of chain in combination with the type of molecular core containing biphenyl near the chiral part.

In this work, we combined a molecular core containing two biphenyls connected by an ester group and a chiral chain with two chiral centres. We present the synthesis and physical properties of new materials with four-phenyl-ring molecular cores laterally substituted by chlorine atoms and a lactic acid unit in the chiral molecular chain. All compounds exhibit TGB phases in a wide temperature range. For most compounds, the TGBC phase is followed by the SmC* phase on cooling.

2. Synthesis

Synthesis of the compounds studied was carried out according to the synthetic path described in Scheme 1. The general chemical formula of the studied materials denoted as ***n*BBL** is shown in the bottom of Scheme 1, n varies from 5 to 12. Both chiral centres have the (S) configuration. The molecular structure of the synthesised compounds was checked using standard analytical methods.

^{1}H-nuclear magnetic resonance (NMR) spectra were acquired on a spectrometer Varian-Gemini 300 HC, with deuterochloroform or dimethyl sulphoxide (DMSO)-d_6 serving as solvent and the signals of the solvent used as internal standards. Chemical shifts are given in the δ-scale (ppm).

2.1 Preparation of (S)-2-methylbutyl-(S)-lactate 1

A solution of 100 g (S)-lactic acid (Lachema, Brno, Czech Republic) and 70.4 g (S)-2-methylbutanol (Merck) in 300 ml of benzene was refluxed using a Dean and Stark trap for 25 h. The benzene was evaporated and the residue was filtered and distilled *in vacuo*, the first fraction being 2-methylbutanol, the second fraction (S)-2-methylbutyl-(S)-lactate ($[\alpha]^{20}_D = -10.5^\circ$ neat). The fraction boiled at 51–54°C/2 torr.

^{1}H-NMR of **1** ($CDCl_3$, 300 MHz): 4.25 (q, 1H, CHOH); 4.0 (m, 2H, $COOCH_2$); 3.3 (brs, 1H, OH); 1.7 (m, 1H, $CH_2\underline{CH}$*); 1.38 (d, 3H, $\underline{CH_3}CHOH$); 1.2 and 1.4 (m, 2H, $\underline{CH_2}CH_3$); 0.9 (m, 6H, $2\times CH_3$).

2.2 Preparation of acid 2

The 4-methoxybiphenyl was chlorinated by sulphurylchloride during boiling for 1 h. The 3-chloro-4-methoxybiphenyl was reacted with acetic acid chloride in the presence of aluminium chloride in 1,2-dichloroethane solution. The resulting acetophenone derivative was converted into acid **2** by the haloform reaction with a total yield of about 60%.

^{1}H-NMR of **2** (DMSO-d_6, 300 MHz): 7.95 (d, 2H, ortho to -COOH); 7.80 (d, 2H, meta to -COOH); 7.78 (d, 1H, ortho to -Cl); 7.7 (dd, 1H, para to -Cl); 7.25 (d, 1H, meta to -Cl); 3.90 (s, 3H, CH_3O).

2.3 Preparation of 4-hydroxy-3-chlorobiphenyl-4′-carboxylic acid 3

The methyl group of acid **2** was removed by boiling in excess hydrobromic acid/acetic acid mixture for several days. Then the reaction mixture was cooled down and poured into water. The resulting 4-hydroxy-3-chlorobiphenyl-4′-carboxylic acid **3** was separated as a yellow powder by suction. The total yield was 95% after crystallisation from a mixture of water/ethanol.

^{1}H-NMR of **3** (DMSO-d_6, 300 MHz): 7.95 (d, 2H, ortho to -COOH); 7.60–7.80 (m, 3H, meta to -COOH and ortho to -Cl); 7.52 (dd, 1H, para to -Cl); 7.1 (d, 1H, meta to -Cl); 10.50 (s, 1H, OH).

2.4 Preparation of phenol 5

Acid **3** was protected by methyl chloroformate using the procedure described in Chin and Goodby [22] and transferred into acyl chloride using thionyl chloride. Then thionyl chloride was evaporated *in vacuo* and the crude chloride was condensed with 2-methylbutyl lactate **1** in pyridine/dichloromethane solution during 20 h under reflux. The reaction mixture was poured into water, extracted by dichloromethane, the combined extracts washed by dilute hydrochloric acid (to remove excess of pyridine) and the water evaporated. The product was stirred in a mixture of tetrahydrofuran and ammonia at room temperature, the reaction was monitored by thin layer chromatography on silica gel. When the reaction was completed the solution was poured into the excess water and extracted by dichloromethane several times. The organic layer was washed by diluted hydrochloric acid, twice washed in water, dried by magnesium sulphate and evaporated to dryness, and washed with hexane. The total yield was about 65%.

^{1}H-NMR of **5** ($CDCl_3$, 300 MHz): 8.12 (d, 2H, ortho to -COO); 7.60 (m, 3H, meta to -COO and ortho to -Cl); 7.42 (dd, 1H, para to -Cl); 7.10 (d, 1H, ortho to -OH); 5.35 (q, 1H, COOC*H); 4.01 (m, 2H, $COO\underline{CH_2}$), 1.7 (m, 1H, $CH_2\underline{C*H}$), 1.65 (d, 3H, $COOCH\underline{CH_3}$); 1.4 and 1.2 (m, 2H, $\underline{CH_2}CH_3$); 0.9 (m, 6H, CH_3).

2.5 Preparation of final products nBBL

The synthesis of 4-alkoxy-3-chlorobiphenyl-4́-carboxylic acids **6** was described in Bubnov *et al.* [21].

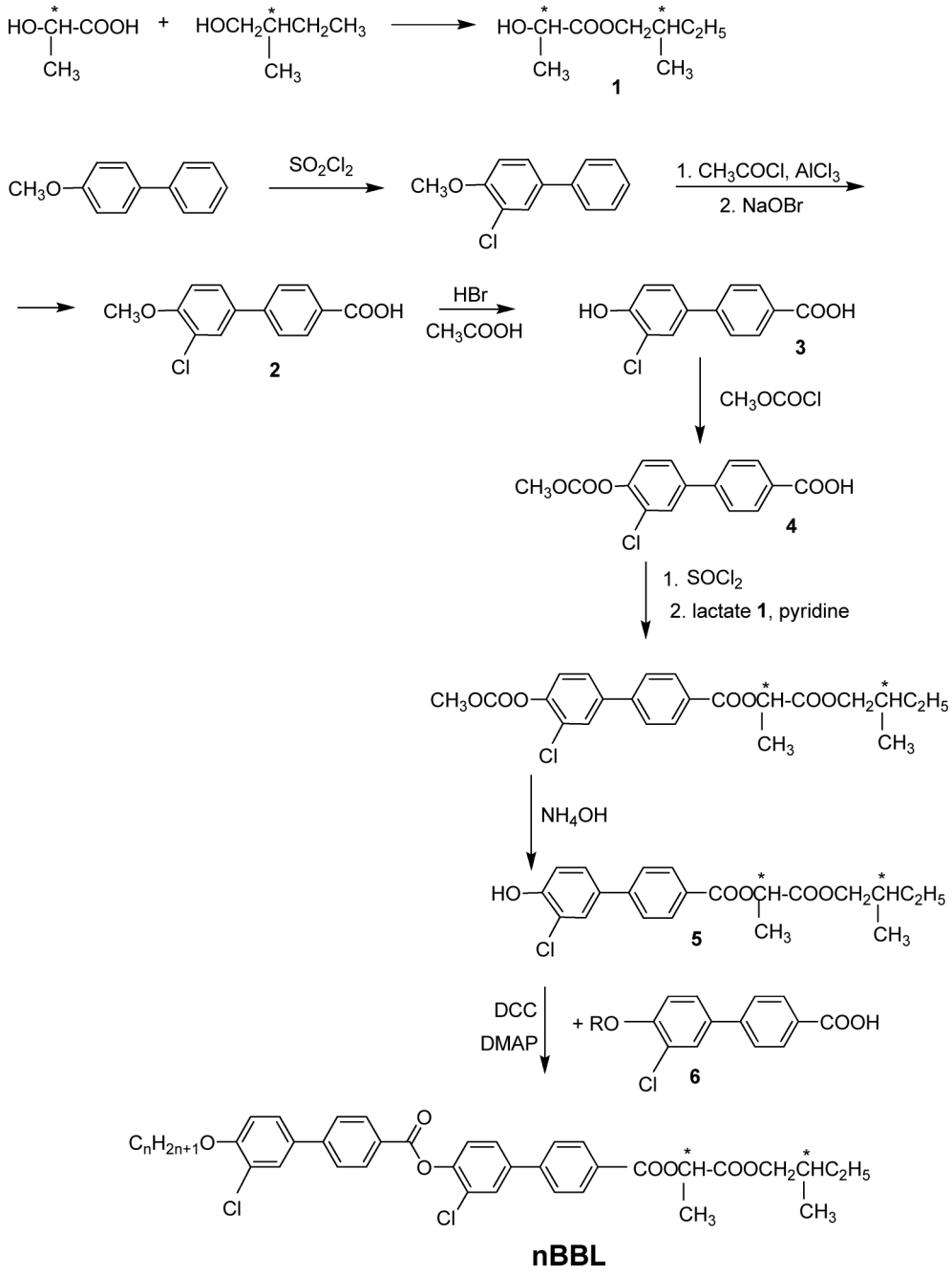

Scheme 1. Synthesis scheme of the compounds studied.

The final products were prepared from **5** and **6** by a standard method of esterification with dicyclohexylcarbodiimide in the presence of dimethylaminopyridine in dichloromethane. All crude products were purified by column chromatography on silica gel using a mixture (99.5:0.5) of dichloromethane and acetone as an eluent and crystallised twice from a mixture of ethanol and acetone. The chemical purity of materials was checked by high performance liquid chromatography, which was carried out using a silica gel column (Bioshere Si 100-5 μm, 4 × 250, Watrex, Prague, Czech Republic) with a mixture of 99.8% toluene and 0.2% methanol as an eluent, and detection of the eluting products by a UV-VIS detector ($\lambda = 290$ nm, which is optimal wavelength for impurity detection). The chemical purity was found to be better than 99.7% under these conditions.

^{1}H-NMR of **8BBL** ($CDCl_3$, 300 MHz): 8.25 (d, 2H, ortho to -COOAr); 8.18 (d, 2H, ortho to -COOC*H); 7.60–7.80 (m, 8H, ortho to -Ar); 7.40 (d, 1H, ortho to

ArCOO-); 7.02 (d, 1H, ortho to -CH_2O); 5.38 (q, 1H, C*HCOO); 4.08 (t, 2H, CH_2OAr); 4.00 (m, 1H, CH_2C*H); 1.87 (quint, 2H, CH_2CH_2OAr); 1.67 (d, 3H, CH_3CH*COO), 1.7 and 1.3 (m, 13H, CH_2, CH); 0.9 (m, 9H, CH_3).

3. Experimental

Phase transition temperatures and enthalpies were determined by differential scanning calorimetry (DSC) studies (Pyris Diamond Perkin-Elmer 7) under cooling and heating runs at a rate of 5 K min^{-1}. The 2–5 mg samples were hermetically sealed in aluminium pans and placed in the calorimeter chamber inflated by nitrogen. The texture observations were performed using a Nikon Eclipse polarising microscope equipped with a Linkam hot stage. The compounds studied were filled by capillarity action in the isotropic phase into cells composed of glass with indium tin oxide (ITO) transparent electrodes (5×5 mm^2). The sample thickness was defined by mylar sheets. Cells with planar and homeotropic orientation and a thickness of 8 μm and 12 μm were used. Free-standing films (FSF) were prepared by spreading melted material over a circular hole (diameter 2 mm) in an aluminium plate.

Spontaneous polarisation, P_S, was determined from hysteresis loops detected during switching in a sinusoidal electrical field of about 20 V μm^{-1} and a frequency of 50 Hz. The spontaneous tilt angle, θ_S, was determined from the angular difference between the extinction positions of structures unwound in opposite DC electrical fields of about ±10 V μm^1.

Frequency dispersion of dielectric permittivity was measured on cooling using a Schlumberger 1260 impedance analyser in a frequency range of 1 Hz to 1 MHz, keeping the temperature of the sample stable during frequency sweeps within ±0.1 K. The frequency dispersion data were analysed using the Cole-Cole formula [14] for the frequency-dependent complex permittivity complemented by second and third terms to eliminate the low frequency contribution from DC conductivity σ and the high frequency contribution due to deficient resistance of the ITO electrodes, respectively:

$$\varepsilon^* - \varepsilon_\infty = \frac{\Delta\varepsilon}{1 + (if/f_r)^{(1-\alpha)}} - i\left(\frac{\sigma}{2\pi\varepsilon_0 f^n} + Af^m\right) \quad (1)$$

where f_r is the relaxation frequency, $\Delta\varepsilon$ the dielectric strength, α the distribution parameter of relaxation, ε_0 the permittivity of a vacuum, ε_∞ the high frequency permittivity and n, m, A are parameters of fitting. Measured real, ε', and imaginary, ε'', part of dielectric permittivity $\varepsilon^*(f) = \varepsilon' - i\varepsilon''$ were simultaneously fitted to Equation (1).

Small angle X-ray diffraction studies were performed using the Bruker Nanostar system (CuKα radiation, Vantec 2000 area detector, MRI TCPU H heating stage) working in the transmission mode and the Bruker GADDS system (CuKα radiation, HiStar area detector) working in the reflection mode. In both systems the temperature stability was 0.1 K. Powder samples for Nanostar were prepared in thin-walled glass capillaries (1.5 mm diameter), partially oriented samples for experiments in reflection were prepared as droplets on a heated surface.

4. Results

4.1 Mesomorphic properties

The phase transition temperatures and enthalpies were determined from DSC and are summarised in Table 1. Some phase transitions, typically between the isotropic and blue phase (BP) and between the TGBC and SmC*phase, could not be detected by DSC because their enthalpy was lower than the sensitivity limit of the DSC apparatus. These transitions, clearly seen in the polarising microscope (see below), are indicated by a star in Table 1. For **10BBL** the DSC plot is shown in Figure 1 as an example. This homologue is the only one for which the phase transition between the BP and the isotropic phase is visible on the DSC plot. Besides the transition peaks, the DSC plot reveals a significant

Table 1. Melting point, phase transition temperatures, T_{tr}, in °C and corresponding enthalpies, ΔH, detected on second temperature run and presented in kJ mol^{-1}.

	Melting point [ΔH]	SmC*	T_{tr} [ΔH]	TGBC	T_{tr} [ΔH]	TGBA	T_{tr} [ΔH]	BP	T_{tr} [ΔH]	Iso
5BBL	50 [+ 4.0]	•	64*	–		•	129 [– 0.11]	–		•
6BBL	75 [+ 8.1]	•	84*	•	96 [– 0.09]	•	126 [– 0.17]	–		•
7BBL	66 [+ 10.4]	•	94*	•	103 [– 0.08]	•	122 [– 0.13]	•	124*	•
8BBL	54 [+ 9.5]	•	98*	•	106 [– 0.08]	•	122 [– 0.16]	•	123*	•
9BBL	51 [+ 6.4]	•	99*	•	106 [– 0.14]	•	119 [– 0.06]	•	121*	•
10BBL	53 [+ 3.6]	•	99*	•	108 [– 0.20]	•	118 [– 0.12]	•	122 [– 0.01]	•
12BBL	50 [+ 8.6]	•	104 [– 0.01]	•	113 [– 0.17]	•	122 [– 0.18]	–		•

* indicates that the phase transition was not recognisable in the differential scanning calorimetry plots and was determined from texture and/or X-ray studies and confirmed by dielectric spectroscopy.

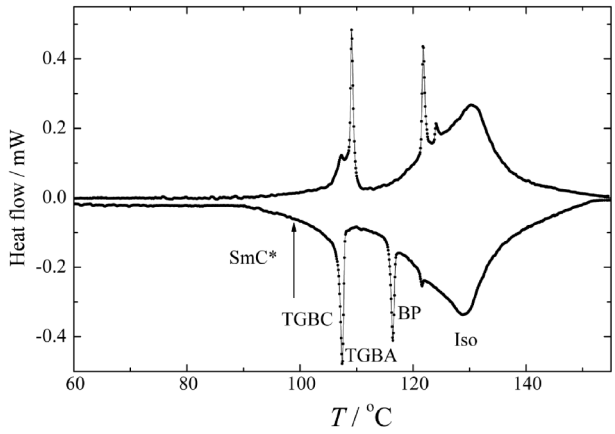

Figure 1. Differential scanning calorimetry plot for **10BBL** taken on second heating (upper) and cooling (lower curve) at a rate of 5 K min^{-1}. Arrow shows the SmC*-TGBC phase transition, which cannot be recognised by this technique (value taken from microscope and/or X-ray temperature dependences). 287×201 mm (600×600 dpi).

broad anomaly within the isotropic phase (Figure 1). Such an anomaly normally occurs in compounds exhibiting TGB phases and is probably connected with pre-transitional effects (see discussion). The anomalies detected at the TGBA-TGBC phase transition are slightly higher than the characteristic values usually found. Nevertheless, some compounds have been reported with comparable high enthalpy values at this phase transition [23,24]. The phase transition between the TGBC and SmC* phases exhibits a strong hysteresis. The SmC* phase exists typically for tens of degrees above the melting point, being wider for longer homologues. This phase can be easily overcooled below room temperature.

The phases (see Table 1) were identified basically from textures observed under polarising microscope and their changes on cooling and/or heating. In samples with planar surface alignment, the TGB phases exhibit a great variety of textures, which are significantly changed at phase transitions. For all the compounds studied a classical blurred coloured fan-shaped texture [25] is mostly observed in the TGBA phase. In Figure 2(a) we show another type of planar texture found in the TGBA phase, which exhibits oily streaks similar to those typical for the cholesteric phase. The oily streaks may persist in the TGBC phase and the birefringence changes with temperature (Figures 2(b) and (c)). At transition to the SmC* phase, a classical fan-shaped texture appears (Figure 2(d)). The onset of the BP is seen in the microscope on cooling from the isotropic phase even though the texture has very low optical contrast (Figure 3(a)). In FSF the texture in TGB phases resembles a fan-shaped texture. In FSF of the TGB phases, the smectic layers are expected to be parallel to the film plane, the TGB blocks being perpendicular to the film surface. Observed FSF textures are presented in Figures 4 and 5 for thin and thick film, respectively. At the transition to the SmC* phase a classical schlieren texture appears (Figure 4(c)).

Under applied electrical field there is no change of the planar texture in the TGBA phase except in the vicinity of the TGBA-TGBC phase transition. Up to 3 K above TGBA-TGBC phase transition temperature, we induced Frederik's transition for DC electrical field higher than 10 V μm^{-1} and specific stripes were observed (Figure 3(b)). The stripes slowly squeeze out after removing the field (Figure 3(c)). When a sufficiently high electrical field is applied in the TGBC phase, transformation into the SmC* phase took place and a fan-shaped texture appeared. After switching off the field, this texture gradually changed back to the TGBC texture within tens of seconds.

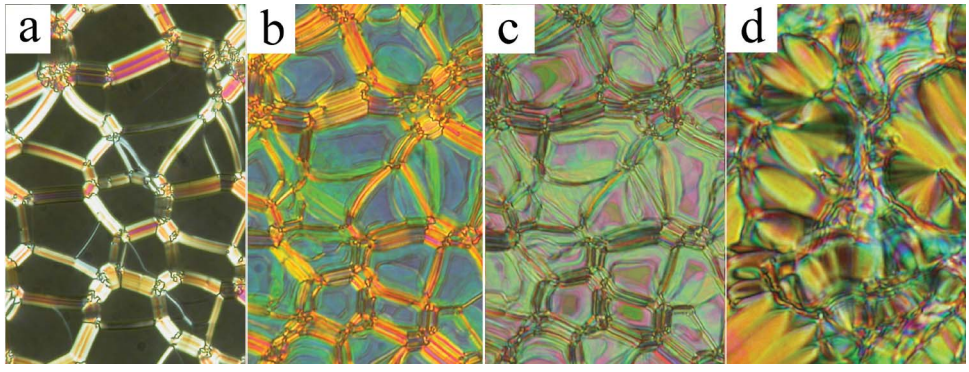

Figure 2. Planar texture of **9BBL** obtained on cooling from the isotropic phase: (a) TGBA phase at $T = 119°C$; (b) TGBC at $T = 106°C$; (c) TGBC at $T = 102°C$; (d) SmC* at $T = 90°C$. The width of the figures corresponds to 200 μm. 320×120 mm^2 (300×300 dpi).

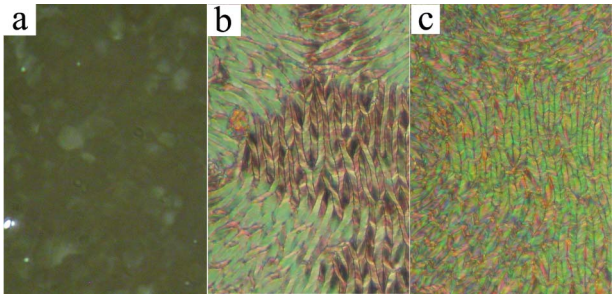

Figure 3. Planar texture of **7BBL** in the: (a) blue phase; (b) TGBA phase at $T = 105°C$ under DC field of about 15 V mm^{-1}; (c) immediately after switching off the field. The width of figures corresponds to 150 μm. 210 × 100 mm^2 (300 × 300 dpi).

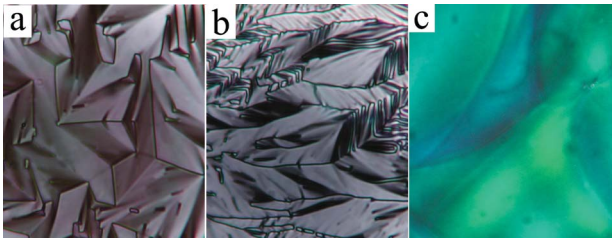

Figure 4. Texture of free-standing film of **10BBL** in the**:** (a) TGBA phase at $T = 115°C$; (b) TGBC phase at $T = 118°C$; (c) SmC* phase at $T = 70°C$. The width of each figure is about 120 μm. 210×80 mm^2 (300×300 dpi).

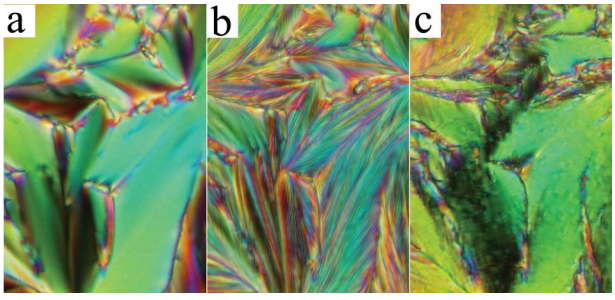

Figure 5. Free standing films of **7BBL** in the: (a) TGBA phase; (b) TGBA-TGBC phase transition; (c) TGBC phase. The figures show evolution of texture at the same sample place. The width of each figure is about 150 μm. 210 × 99 mm^2 (300 × 300 dpi).

4.2 *Spontaneous values*

Ferroelectric switching has been detected in the TGBC and SmC* phases and temperature dependences of spontaneous polarisation and spontaneous tilt angle have been measured (see Figure 6). Both quantities exhibit a significant jump at the transition from the TGBA phase evidencing about character of first order transition. Both quantities exhibit no anomaly at the

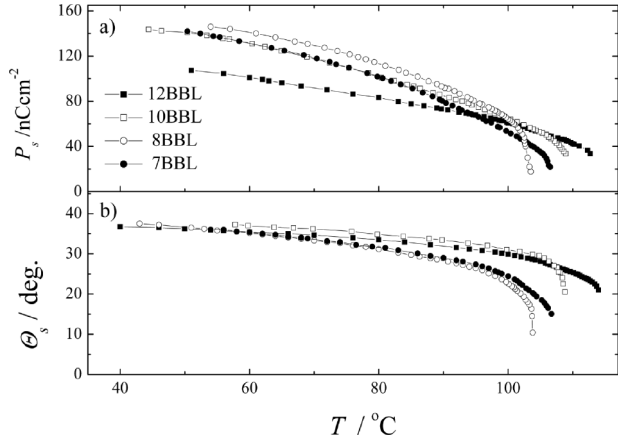

Figure 6. Temperature dependence of (a) spontaneous polarisation and (b) spontaneous tilt angle for indicated compounds. 287 × 201 mm^2 (600×600 dpi).

border of both phases as the TGBC phase is transformed into the SmC* phase under the measuring field and thus the transition is removed. The values of spontaneous tilt at saturation reach relatively high values (up to 40). The coercive switching field increases on cooling probably because of an increase of viscosity and in the overcooled state it exceeded the parameters of our apparatus (150 V), which made it impossible to measure down to room temperature.

4.3 *X-ray measurements*

From X-ray diffraction measured at a range of small scattering angles the layer spacing, *d,* was evaluated in the smectic phases (see Figure 7). In the TGBA phase, *d* is nearly temperature independent. On cooling within the tilted phases the decrease of *d* is in

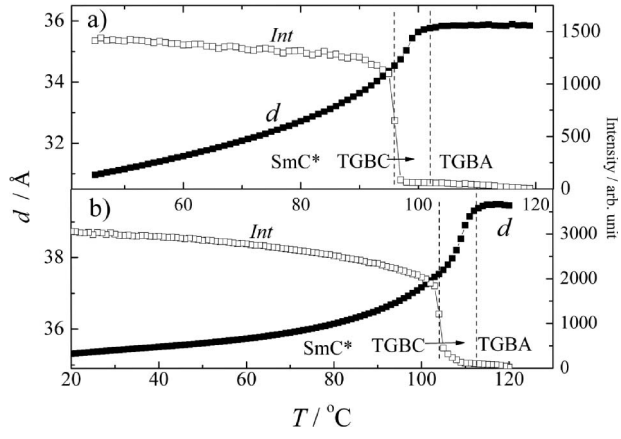

Figure 7. For compounds (a) **7BBL** and (b) **12BBL** temperature dependences of layer spacing, *d*, calculated from the position of X-ray peak and intensity of the X-ray signal measured on cooling. 287×201 mm^2 (600×600 dpi).

agreement with the increasing tilt angle. The scattering intensity exhibits low values in both TGB phases and increases at the transition to the SmC* phase. The increase of intensity at the TGBC-SmC* phase transition is related more to the improvement of sample alignment than to phase structure. It is necessary to point out that the X-ray peak detected in both TGB phases is significantly sharper than a signal that may be detected in the nematic (cholesteric) phase and evidencing a short-range smectic order. Additionally, such a weak signal is expected only in a narrow temperature interval above phase transition to a smectic phase. The width of signal in **BBL** compounds points to long-range smectic ordering.

4.4 Dielectric spectroscopy

The frequency dispersion of complex permittivity was measured at stabilised temperatures over a wide temperature range of the TGBA, TGBC and SmC* phases. Within these phases only one relaxation was detected in the studied frequency range of 10 Hz–1 MHz. A three-dimensional plot of the imaginary part of dielectric permittivity versus temperature is shown in Figure 8 for **6BBL**. The dielectric spectroscopy data were fitted with Equation (1), which yielded the temperature dependence of the dielectric strength, $\Delta\varepsilon(T)$, and relaxation frequency, $f_r(T)$. The behaviour of both quantities was qualitatively the same for all of the studied homologues. For **7BBL** and **10BBL** temperature profiles of $\Delta\varepsilon(T)$ and $f_r(T)$ are shown in

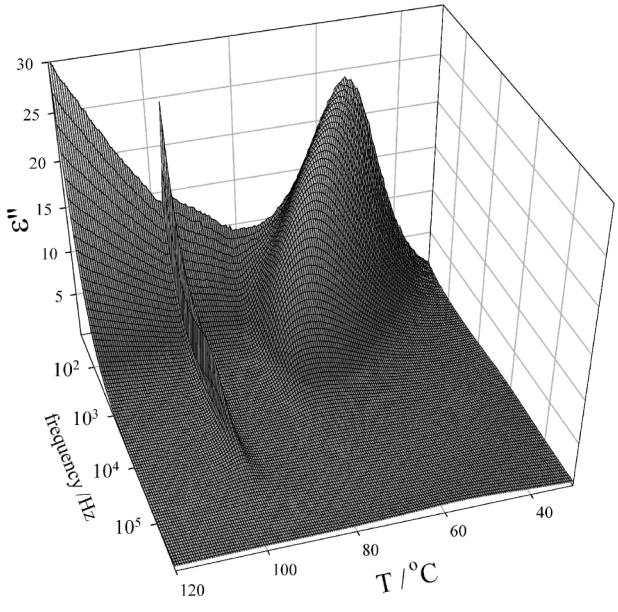

Figure 8. Three-dimensional plot for the imaginary part of permittivity in the frequency range 10–10^6 Hz for **6BBL**. 558 × 520 mm^2 (150 × 150 dpi).

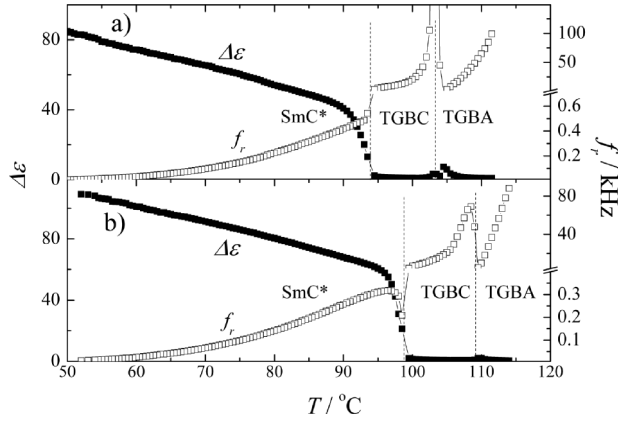

Figure 9. Temperature dependences of fitted $\Delta\varepsilon$ and f_r for (a) **7BBL** and (b) **10BBL**. 287×201 mm^2 (600×600 dpi).

Figure 9. $\Delta\varepsilon$ exhibits a small peak at the TGBA-TGBC phase transition and a strong increase when entering the SmC* phase followed by a linear increase on cooling within the SmC* phase. The relaxation frequency exhibits a linear decrease on cooling within the TGBA phase, which implies the typical behaviour of the soft mode (amplitude fluctuations of the director) expected in this phase [15]. Freezing of this mode at the TGBA-TGBC transition is the origin of the molecular tilt in the TGBC phase. In the TGBC phase f_r of the soft mode steeply increases and its $\Delta\varepsilon$ decreases on cooling and thus the soft mode is overwhelmed by a lower frequency mode, namely azimuthal fluctuations of the tilted director [15]. In the SmC* phase the classical Goldstone mode occurs with much lower relaxation frequency and higher strength compared with the modes existing in both TGB phases. When comparing properties of modes of each individual homologue, it can be seen that the relaxation frequencies are considerably higher for shorter homologues while the dielectric strength does not differ significantly (see Figure 9).

5. Discussion and conclusions

A series of compounds was prepared with molecular cores consisting of two biphenyls laterally substituted by chlorine, the chiral chain with two lactate units, and an alkoxy chain containing $n = 5$–12 carbons. All these compounds exhibit TGBA and SmC*phases. The TGBC phase existed in all studied homologues except for $n = 5$, in which the TGBA phase was 65 K broad. It is the widest TGB phase ever found. For the other homologues the TGBA phase is also relatively broad, becoming gradually narrower from 30 to 9 K for n increasing from 6 to 12. Thus the temperature range of the TGBA phase can be effectively tuned by

prolongation of the alkoxy chain. For $n = 7$–10, the BP 1 to 3 K broad exists above the TGBA phase. The occurrence of this phase provides evidence of high chirality of the studied mesogens. The SmC* phase exists for more than 40 K above the melting point in homologues with $n = 8 \div 12$. Moreover, this phase may be overcooled by about a further 30 K and thus exists below room temperature. For shorter homologues the SmC* phase is narrower, but still relatively wide. In the isotropic phase a pre-transitional behaviour is found, manifested by a rather strong diffuse anomaly in the DSC plot. Such a type of anomaly can be detected in compounds exhibiting the TGB phases [26–28]. In Goodby *et al.* [26], pre-transitional effects in the isotropic phase, namely evolution of a short-range SmA order in the form of cybotactic groups surrounded by normal liquid or, on the other hand, a network of screw dislocation floating in an amorphous liquid, are considered as an origin of this anomaly [26, 27]. An ordering similar to that in the blue fog phase (BP III) is given as an alternative explanation of the 'intermediate state' between the classical isotropic phase and TGB phase (resp. BP). In Navailles *et al.* [8], a diffuse anomaly was also found in the cholesteric phase accompanied by the TGB phase. That anomaly was explained by evolution of a short-range TGB structure within the cholesteric phase.

The planar texture of TGB phases (molecules generally parallel to the sample plane) is often blurred with colour related to the selective refraction on the helical superstructure with the axis parallel to the sample plane (Figure 2). Thus the helical superstructure plays a similar role to the helix in cholesterics with the axis perpendicular to the director [16]. On the other hand in FSF, where molecules are perpendicular to the film plane (the axis of the helical superstructure lying in the film plane), a texture very similar to fan-shaped is formed (see Figures 4 and 5). In FSF, the helical superstructure adopts the role of layers in smectic phases. The helical superstructure cannot exist without a lattice of TGBs consisting of array of screw dislocations. Under a sufficiently high DC electrical field these boundaries are removed, the SmC* phase being formed. The spontaneous reconstruction of these boundaries after the field is switched off takes tens of seconds. The intensity of X-rays scattered on the smectic layers is much lower in TGB phases compared with the SmC* phase, which reflects disorder due to defect boundaries.

Dielectric spectroscopy reveals the soft mode in the TGBA phase and the Goldstone mode in the TGBC phase. These modes are active in the individual blocks that form the superstructure. It can be expected that each of these modes is not uniform within the blocks, as the vibrations are clamped at the grain boundaries. It results in a twist deformation of the director inside the blocks [15]. The elastic force connected with this deformation reduces the dielectric strength of both soft and Goldstone modes and increases their relaxation frequency. From a theoretical model it follows that for the power of this effect the molecular anchoring at the grain boundaries, twist elastic constant of the material and block width plays a role [15]. Comparing our data for the Goldstone mode in TGBC and SmC* phases near the phase transition it can be seen that the dielectric strength is, by two orders, higher and relaxation frequency lower in the SmC* phase. As for the soft mode in the TGBA phase, a direct comparison was not possible as the SmA phase was not present in the compounds studied.

To summarise, using dielectric spectroscopy and X-ray diffraction measurements, we investigated TGBA, TGBC and SmC* phase properties. We confirmed the sequence of phases and established structural parameters from X-ray data and characteristics of modes observed by dielectric spectroscopy.

Acknowledgements

This work was supported by projects IAA100100710 and IAA100100911 (Grant Agency of AS CR), by Research Project AVOZ 10100520 and Grant No. 202/09/0047 from the Grant Agency of the Czech Republic. The X-ray diffraction measurements were performed at the Structural Research Laboratory, Chemistry Department, University of Warsaw, Poland, which was established with financial support from the European Regional Development Fund, Project No: WKP 1/1.4.3./1/2004/72/72/165/2005/U.

References

[1] Renn, S.R.; Lubensky, T.C. *Phys. Rev. A Gen. Phys.* **1988**, *38*, 2132–2147.
[2] Oswald, P.; Pieranski, P. *Smectic and Columnar Liquid Crystals*; CRC Press: New York, 2006.
[3] Kitzerow, H.-S.; Bahn, Ch. *Chirality in Liquid Crystals*; Springer-Verlag: Heidelberg, 2001.
[4] Lubensky, T.C.; Renn, S.R. *Phys. Rev A Gen. Phys.* **1990**, *41*, 4392–4401.
[5] Goodby, J.W.; Waugh, M.A.; Stein, S.M.; Chin, E.; Pindak, R.; Patel, J.S. *Nature* **1989**, *337*, 449–452.
[6] Nguyen, H.T.; Bouchta, A.; Navailles, L.; Barois, P.; Isaert, N.; Twieg, R.T.; Maaroufi, A.; Destrade, C. *J. Phys. II France* **1992**, *2*, 1889–1906.
[7] Brunet, M.; Navailles, L.; Clark, N.A. *Eur. Phys. J. E. Soft Matter* **2002**, *7*, 5–11.
[8] Navailles, L.; Garland, C.W.; Nguyen, H.T. *J.Phys. II France* **1996**, *6*, 1243–1258.
[9] Ribeiro, A.C.; Oswald, L., Nicoud, J.F.; Soldera, A.; Guillon, D.; Galerne, Y. *Eur. Phys. J. B.* **1998**, *1*, 503–512.
[10] Lukyanchuk, I. *Phys. Rev. E* **1998**, *57*, 574–581.
[11] Galerne, Y. *Eur. Phys. J. E. Soft Matter* **2000**, *3*, 355–368.

[12] Dodge, M.R.; Vij, J.K.; Cowling, S.J.; Hall, A.W.; Goodby, J.W. *Liq. Cryst.* **2005**, *32*, 1045–1051.
[13] Xu, H.; Panarin, Y.P.; Vij, J.K.; Seed, A J.; Hird, M.; Goodby, J.W. *J. Phys. Condens Matter* **1995**, *7*, 7443–7452.
[14] Pandey, M.B.; Dhar, R.; Kuczynski, W. *Ferroelectrics* **2006**, *343*, 69–82.
[15] Ismaili, M.; Bougrioua, F.; Isaert, N.; Legrand, C.; Nguyen, H.T. *Phys. Rev. E* **2001**, *65*, 011701–1–15.
[16] Kašpar, M.; Hamplová, V.; Novotná, V.; Glogarová, M.; Pociecha, D.; Vaněk, P. *Liq. Cryst.* **2001**, *28*, 1203–1209.
[17] Novotná, V.; Kašpar, M.; Hamplová, V.; Glogarová, M.; Bílková, P.; Domenici, V.; Pociecha, D. *Liq. Cryst.* **2008**, *35*, 287–298.
[18] Hsieh, W.-J.; Wu, S.-L. *Mol. Cryst. Liq. Cryst*. **1997**, *302*, 253–269.
[19] Hamplová, V.; Bubnov, A.; Kašpar, M.; Novotná, V.; Lhotáková, Y.; Glogarová, M. *Liq. Cryst.* **2003**, *30*, 1463–1469.
[20] Hamplová, V.; Bubnov, A.; Kašpar, M.; Novotná, V.; Glogarová, M. *Liq. Cryst.* **2003**, *30*, 493–497.
[21] Bubnov, A.; Hamplová, V.; Kašpar, M.; Glogarová, M.; Vaněk, P. *Ferroelectrics* **2000**, *243*, 27–35.
[22] Chin, E.; Goodby, J.W. *Mol. Cryst. Liq. Cryst*. **1986**, *141*, 311–320.
[23] Nguyen, H.-T.; Ismaili, M.; Isaert, N.; Achard, M.F. *J. Mater. Chem.* **2004**, *14*, 1560–1566.
[24] Li, M.-H.; Laux, V.; Nguyen, H.-T.; Sigaud, G.; Barois, P.; Isaert, N. *Liq. Cryst.* **1997**, *23*, 389–408.
[25] Dierking, I. *Textures of Liquid Crystals*; Wiley-VCH: Weinheim, 2003.
[26] Goodby, J.W.; Slaney, A.J.; Booth, C.J.; Nishiyama, I.; Vuijk, J.D.; Styring, P.; Toyne, K.J. *Mol. Cryst. Liq. Cryst*. **1994**, *243*, 231–298.
[27] Jameé, P.; Pitsi, G.; Li, M.-H.; Nguyen, H.-T.; Sigaut, G.; Thoen, J. *Phys. Rev. E* **2000**, *62*, 3687–3693.
[28] Kašpar, M.; Novotná, V.; Hamplová, V.; Pociecha, D.; Glogarová, M. *Liq. Cryst.* **2008**, *35*, 975–985.